Available online at www.sciencedirect.com
SCIENCE DIRECT®
Biomaterials 27 (2006) 1223–1235
Biomaterials
www.elsevier.com/locate/biomaterials

Porous Ti_6Al_4V scaffold directly fabricating by rapid prototyping: Preparation and in vitro experiment

Jia Ping Li[a,b,d,*], Joost R. de Wijn[a], Clemens A. Van Blitterswijk[a], Klaas de Groot[a,c]

[a]*Institute for Biomedical Technology, Twente University, Prof. Bronkhorstlaan 10-D, 3723 MB Bilthoven, The Netherlands*
[b]*Porogen, B.V, Enschede, The Netherlands*
[c]*CAM Implants, Zernikedreef 6, 2333CL, Leiden, The Netherlands*
[d]*School of Mechanical Engineering & Automation, BeiHang University, Beijing, China*

Received 24 March 2005; accepted 23 August 2005
Available online 5 October 2005

Abstract

Three-dimensional (3D) fiber deposition (3DF), a rapid prototyping technology, was successfully directly applied to produce novel 3D porous Ti_6Al_4V scaffolds with fully interconnected porous networks and highly controllable porosity and pore size. A key feature of this technology is the 3D computer-controlled fiber depositing of Ti_6Al_4V slurry at room temperature to produce a scaffold, consisting of layers of directionally aligned Ti_6Al_4V fibers. In this study, the Ti_6Al_4V slurry was developed for the 3D fiber depositing process, and the parameters of 3D fiber depositing were optimized. The experimental results show how the parameters influence the structure of porous scaffold. The potential of this rapid prototyping 3DF system for fabricating 3D Ti_6Al_4V scaffolds with regular and reproducible architecture meeting the requirements of tissue engineering and orthopedic implants is demonstrated.

Keywords: Titanium alloy; Porosity; Scaffold; Rapid prototyping-three-dimensional fiber deposition

1. Introduction

Scaffolds are of great importance for tissue engineering and orthopedic implants because they enable to provide biological anchorage for the surrounding bony tissue via the ingrowth of mineralized tissue into the pore space [1]. These scaffolds require a specific external shape and a well-defined internal structure with interconnectivity [1–3]. Recently, porous ceramics and polymers have been extensively studied to promote bone or tissue ingrowth into pores [4–9]. However, ceramics and polymers are not very strong and can easily transform [10,11], they are less appropriate in load-bearing applications, such as in spinal interbody fusion. Therefore, metals like titanium and its alloys are widely used for orthopedic and dental implants [12]. They possess low density, good mechanical properties (elastic modulus, toughness, and fatigue strength) and biological and chemical inertness. Recently, there has been an increasing interest in fabricating porous titanium scaffold for bone tissue engineering [13–15]. Porous titanium and its alloys have been used in dental and orthopedic applications since the end of 1960s [16–18]. Many available methods for producing porous titanium and titanium alloy scaffolds include sintering together of the particles [19] or plasma spraying of the powder on a dense substrate followed by the cutting of the porous layer [20], compressing and sintering of titanium fibers [21,22], solid-state foaming by expansion of argon-filled pores [23] and polymeric sponge replication [24]. However, none of these conventional techniques has allowed for building scaffolds with a completely controlled design of the external shape as well as of the interconnected pore network. The imperfection of the conventional techniques has encouraged the use of a rapid prototyping (RP) technology [25]. Since 1980s RP technologies have emerged

*Corresponding author. Institute for Biomedical Technology, Twente University, Prof. Bronkhorstlaan 10-D, 3723 MB Bilthoven, The Netherlands. Tel.: +31 30 2295289; fax: +31 30 2280255.
E-mail address: j.li@tnw.utwente.nl (J.P. Li).

0142-9612/$ - see front matter © 2005 Elsevier Ltd. All rights reserved.
doi:10.1016/j.biomaterials.2005.08.033

as a revolutionary manufacturing process with inherent capability to rapidly make objects in virtually any shape. RP, combining computer-aided design (CAD) with computer-aided manufacturing (CAM), has the distinct advantage of being able to build objects with predefined microstructure and macrostructure [26,27]. This distinct advantage gives RP the potential for making scaffolds or orthopedic implants with controlled hierarchical structures [28–33]. Until now RP developments mainly focused on polymer and ceramic materials [34–39]. The transfer of RP technologies to metal materials for tissue engineering and orthopedic implants possesses a significant challenge. There are few investigators on making metal scaffold for orthopedic and tissue engineering application by rapid prototyping techniques [3,40,41]. Two methods were applied to make metal scaffold. One is indirect to make porous scaffolds by invest casting melt metal or metal powder slurry into a mold where the mold was made using RP [40–42], in addition to indirect processing, other researchers have been developing porous titanium scaffolds for tissue engineering using direct metal deposition [3,43,44].

Here, we report the first example of RP Ti_6Al_4V scaffold with self-supporting features fabricated directly by 3D fiber deposition. In this paper, we investigated the design and fabrication of 3D Ti_6Al_4V scaffolds and performed in vitro studies to assess cell attachment, cell proliferation and differentiation of the scaffolds.

2. Materials and methods

2.1. Materials

- Ti_6Al_4V powders with a mean particle diameter of 45 μm (Bongen Titanium (China) Co, ltd) were used in this study. The particles are spherical in shape.
- Methylcellulose (MC, Fisher Scientific B.V) and stearic acid (Acros organics, USA) were used as binder and dispersant.

2.2. Methods

2.2.1. Preparation of the Ti_6Al_4V slurry

The Ti_6Al_4V slurry was prepared as follows: The Ti_6Al_4V powder (66 vol%) was mixed with an aqueous solution of methylcellulose and stearic acid (34 vol%). The slurry was stirred for 1 h at room temperature (RT) to obtain homogenous slurry.

The concentration of the Ti_6Al_4V powder in the slurries has influence on the viscosity of the slurry. The effect of powder concentration was studied by utilizing the slurries with Ti_6Al_4V powder concentrations ranging from 64 to 68 vol%. A powder concentration of 66 vol% was used for most studies unless otherwise specified.

2.2.2. 3D fiber deposition

As a 3D fiber depositing device, the "Bioplotter" was used, which has been reported by Landers and Mülhaupt [45,46]. Fig. 1A shows the system, consisting of: (1) a Ti_6Al_4V slurry dispensing unit consisting of a syringe and nozzle; (2) air pressure plunger to regulate flow of slurry; (3) positional control unit linked to a personal computer containing software (PrimCAM) for generating fiber deposition paths.

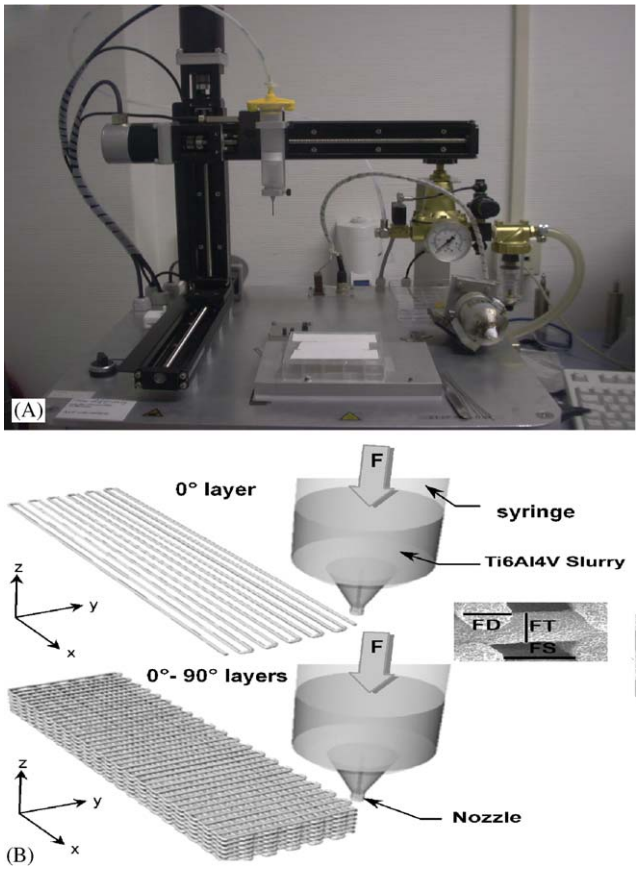

Fig. 1. 3D fiber depositing system. (A) 3D fiber depositing system, (B) 3D fiber depositing scaffold process.

2.2.3. Scaffold development

The Ti_6Al_4V slurry was placed in a plastic syringe, through a fixation unit mounted on the "*Y*"-axis of the apparatus and kept at RT. Air pressure (*P*) was applied to the syringe through a pressurized cap. Rectangular block models were loaded on the Bioplotter CAM software. The process involved depositing continuous fibers of material to produce two-dimensional (2D) layers with alternating 0°/90° lay-down patterns of finite thickness and then building the 3D scaffold up layer-by-layer. Fig. 1B shows the processing of 3D fiber depositing porous Ti_6Al_4V scaffold.

The nozzle used to extrude Ti_6Al_4V slurry fibers is a stainless steel hypodermic needle. The nozzle size is expressed as inner diameter of the nozzle, and a length of 16.1 mm. A nozzle diameter of 400 μm was used for most studies unless otherwise specified. For all the experiments addressed, fiber spacing was set to 0.5 mm to create pore size around 400 μm since pore size around this range assure a rich blood supply, nutrient and waste exchange and promote in growth of bone [47–49], and the thickness between fiber layers was kept at 0.35 mm which is about 0.85* nozzle size as discussed previously [46].

After fiber depositing the samples were first dried for 24 h at RT, then dried for 24 h at 50 °C, and finally sintered in a high vacuum furnace (10^{-5} mbar) applying a heating profile as follows:

RT 600 min → 500 °C 450 min → 1250 °C 120 min
→ 1250 °C furnace cooling → 25 °C.

2.2.4. Optimization of 3D fiber depositing parameters for fabrication scaffold

The principle of 3D fiber deposition is similar to that of fused deposition modeling (FDM). Many groups have applied FDM to fabricate scaffold for tissue engineering [10,50–52]. The optimized FDM

process involves complex interactions between the hardware, software and material properties as discussed previously [39,53,54]. Before fabricating a 3D Ti_6Al_4V scaffold, experiments were focused on understanding the influence of concentration of powder, air pressure, the feeding speed of fiber depositing and the initial height of fiber depositing on the output quality of the processed scaffold. These four primary parameters, together with the experimented values in brackets, include: (1) the concentration of Ti_6Al_4V powder; (2) the fiber depositing pressure, P (i.e. 2, 2.5 and 3 bars); (3) the speed of feeding, S (i.e. 210, 280, 350 and 420 mm/min); and (4) the initial height of fiber depositing (i.e. initial distance between the tip and the platform), H (i.e. 0.1, 0.25 and 0.4 mm). Different scaffolds were produced at various settings.

2.2.5. Characterization

The shape of Ti_6Al_4V powders was analyzed by environmental scanning electron microscope (ESEM, XL-30, Philips, Eindhoven, The Netherlands). Particle size distributions were measured by Retsch Technology in Germany, using a CRYSTALSIZER® which is based on using incoherent light diffraction.

The rheological behavior of Ti_6Al_4V slurries was measured at room temperature by viscometer (Brookfield engineering labs DV-II+ viscometer) with interval time at a speed of 10 rpm with a RV0 spindle.

The dispensability of Ti slurry was measured in terms of flow rate. Flow rate can be defined as weight of slurry extruded from nozzle per minute. The average of 3 measurements was used to represent the flow rate at experimental machine setting.

3D fiber depositing scaffolds were characterized under ESEM to measure the diameter of fiber and to select the potential settings of fiber depositing parameters. Since the primary concern was to produce consistent and uniform fibers, the fiber diameter (FD) from nozzle, the spreading tendency (standard deviation) of the fiber spacing (FS) and thickness of the fibers (FT) produced by the potential settings were then measured and compared to pick out an optimized setting of parameters (shown in Fig. 1B).

The porosity of the Ti_6Al_4V scaffolds was calculated from the ratio of weight and volume by comparing the bulk density of samples ($n = 10$) with the theoretical density of Ti_6Al_4V: 4.45 g/cm^3.

Five samples from each kind of scaffold produced at various settings for the fiber depositing air pressure and feeding speed were randomly chosen. Compression tests of porous Ti_6Al_4V samples ($4 \times 4 \times 6$ mm, $n = 5$) were performed at room temperature with a crosshead speed of 1 mm/min (Zwick/Z050, Germany). The loading direction is in the Z-direction of the deposition process.

2.2.6. In vitro experiment

2.2.6.1. Cell attachment and proliferation. MC3T3-E1 osteoblast-like cells were used for the cell attachment study. The culture medium used was α-MEM supplemented with 10% fetal bovine serum (FBS, Life Technologies, The Netherlands), antibiotics, and 1% sodium pyruvate. The cells were seeded on porous Ti_6Al_4V samples placed in a 25-well plates at 0.6×10^6 cells/per sample in 4 ml of medium, and cultured at 37 °C in a humidified atmosphere with 5% CO_2 and 95% air. After being cultured for 1, 3 and 7 days, respectively, the samples ($n = 2$) were fixed and then rinsed with PBS, dehydrated in a graded ethanol series, critical point dried, sputter coated with carbon and examined with ESEM. Other samples ($n = 3$) were digested with proteinase K (Sigma, The Netherlands), added with heparin (Leo Pharm, The Netherlands) and Ribonu-clease A (Sigma, The Netherlands), then shaken and incubated at 56 °C for 16 h. A volume of 100 μl solution of each sample was mixed with 100 μl Cyquant GRDye (Molecular Probe, Poland), and the fluorescence was measured with fluorimeter (Perkin Helmer) at emission wavelength 520 nm and excitation 480 nm. The DNA content of cells attached on the porous samples was counted through a pre-made standard DNA curve.

2.2.6.2. ALP/DNA analysis. The alkaline phosphatase (ALP) activity expressed as a function of cell DNA content was determined using the Cyquant kit (Molecular Probes, C7026, Leiden, The Netherlands). After 3 and 7 days cultured in the presence of dexamethasone, 3 cell-seeded samples were washed with Phosphate Buffered Saline (PBS; Life Technologies) and stored at −80 °C for at least 24 h. After thawing on the ice, the cells were sonicated (Branson 250) in PBS with 0.2% Triton X-100 (Sigma) for 10 s. The supernatant was employed for the determination of ALP activity according to Lowry's method [55] using ρ-nitrophenyl phosphate (Merck, Germany). A volume of 100 μl solution of each sample was mixed with 100 μl Paranitrophenyl phosphate substrate (Sigma) solution on 96-well microplate reader, and then ALP activity was assayed by measuring the mount of release of ρ-nitrophenol from ρ-nitrophenyl phosphate as previous described [56,57]. A standard curve was generated using known concentrations of ρ-nitrophenol. All samples and standards were measured on a BIO-TEK automated microplate reader (New York, USA) at 405 nm. To measure the DNA contents, a cyquant assay kit (Molecular Probes) and a LS-50B fluorimeter were used.

2.2.6.3. Protein content of cells layers. The protein content of cell layers was determined using a commercially available kit (Micro/Macro BCA, Pierce chemical Co, Rockford, IL, USA) as previously described [58]. The assay was performed within 96-well microreader plates. The absorbance at a wavelength of 570 nm being monitored using a microplate reader (Dynatech, MR 7000, Billinghurst, UK). Bovine serum albumin was used as standard.

3. Results

3.1. Ti_6Al_4V powder and slurry

Fig. 2A illustrates an image of Ti_6Al_4V powder under ESEM. It shows that the particles have both a highly spherical shape and smooth surface. The distribution of the particle size of Ti_6Al_4V powder is given in Fig. 2B, the majority (~50%) being in the range of 10–30 μm. Of significant importance for the 3D fiber deposition of Ti_6Al_4V scaffolds are the rheological properties of the slurry. Landers reported the rheological properties must be balanced to achieve flow during dispensing and preferably high thixotropy [59]. Fig. 3 shows the viscosity as function of time. The viscosity of slurries with different powder concentrations is shown in Fig. 3A. It can be seen that the viscosity decreases with increasing time, revealing the slurry is non-Newtonian. When the measurement is repeated on slurry with a concentration of 66 vol% after 20 min, the same tendency of decreasing viscosity is observed (Fig. 3B). The experimental result reveals that the slurry displays a thixotropic behavior [60]. A reduction in viscosity occurs when shaken, stirred, or otherwise mechanically disturbed, but at rest the slurry recovers in time, eventually reaching its original viscosity.

3.2. Concentration of powder

The viscosity is related to the concentration of the powder in the slurry while binder is at a constant concentration. The higher the powder concentration, the higher the viscosity is. Apparently, a lower viscosity will result in deformation of the deposited fiber, and a higher viscosity of a material will cause a greater resistance against flowing and affect the quality of scaffold. The powder concentration is an important factor which affects the

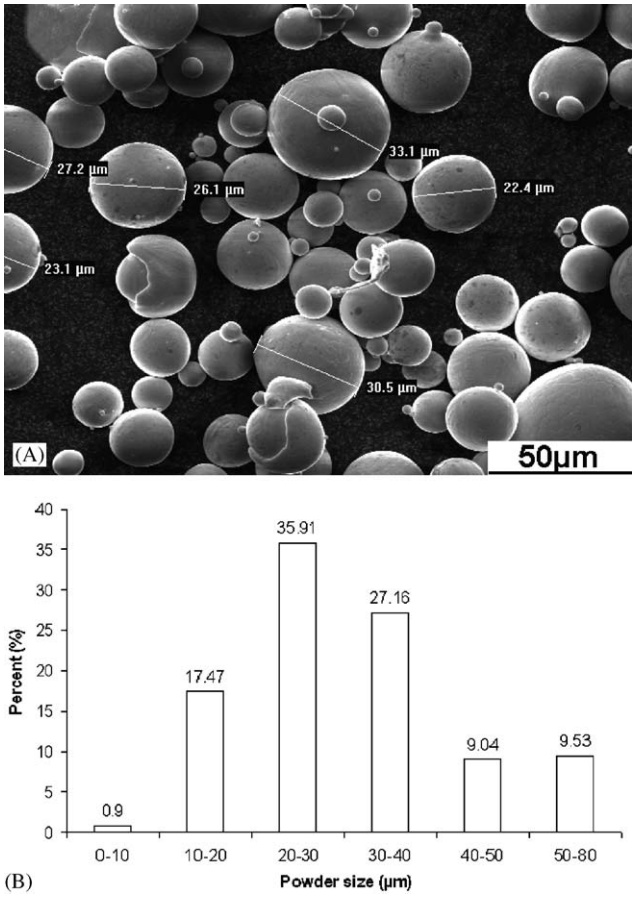

Fig. 2. Ti_6Al_4V powder. (A) morphology of powder, (B) distribution of powder.

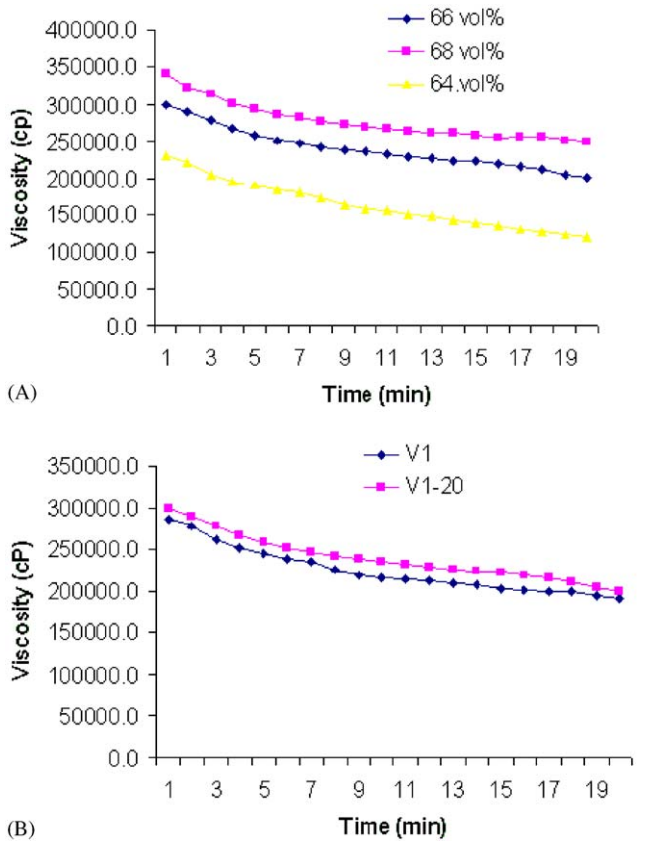

Fig. 3. (A) Viscosity of Ti_6Al_4V slurry with different concentration of powder. (B) Viscosity of slurry with 66 vol% concentration, V1-20 means measurement after 20 min of the first measurement.

architecture of scaffold, as reflected in Fig. 4. It can be seen that the use of a low concentration of powder has undesirably resulted in gravity-induced flow subsequent to depositing (Fig. 4A). Where slurry with a high concentration of 68 vol% was used, there is little or no attachment between the layers (Fig. 4C). Slurry with a concentration of 66 vol% shows a good attachment between layers (Fig. 4B), and has a consistency high enough to withstand flow under its own weight. Therefore, slurry with a concentration of 66 vol% was applied for later experiment.

3.3. Viscosity, nozzle diameter and air pressure on the flow rate

The fiber extruded from the FDM nozzle depends on the viscosity of material, the nozzle diameter and geometry, the pressure drop (ΔP) and the flow rate [61–63]. For Newtonian behavior of a fluid, the Hagen–Poiseuille equation expressed that the flow rate of a fluid through a circular tube (such as a nozzle) as [64]:

$$Q = \frac{\pi \Delta P}{128 L \eta} d^4,$$

where Q is the flow rate of fluid through the nozzle direct (diameter d and length L), η is the viscosity of the fluid, and ΔP is the pressure between the tip of the nozzle and the fluid in the syringe. It can be seen that the flow rate of such a fluid is directly proportional to the pressure across the syringe and nozzle tip at constant nozzle diameter (d), and inversely proportional to nozzle length (L) and viscosity (η). Different nozzles were used to determine the flow rate as a function of viscosity, nozzle size and pressure. In Fig. 5A–C the increased flow rate is plotted against P, d^4 and $1/\eta$, respectively, showing non linearity except possibly at the lowest flow rate. As can be expected, the behavior of the slurry is non-Newtonian.

It is of importance to control flow rate of slurry. If the flow rate is too high, over-deposition of the fiber, causing draping between fibers and reducing porosity will occur. On the other hand, if Q is too low, this will reduce the fiber diameter at a certain feeding speed, thus forming less contact area between the underlying fibers and affecting the strength of scaffold. In our study, a stainless needle shaped nozzle was used to prevent the depositing material from adhering and accumulating around its tip during fiber deposition. The air regulator was used to vary and set the applied pressure for fiber deposition while the PrimCAM software was used

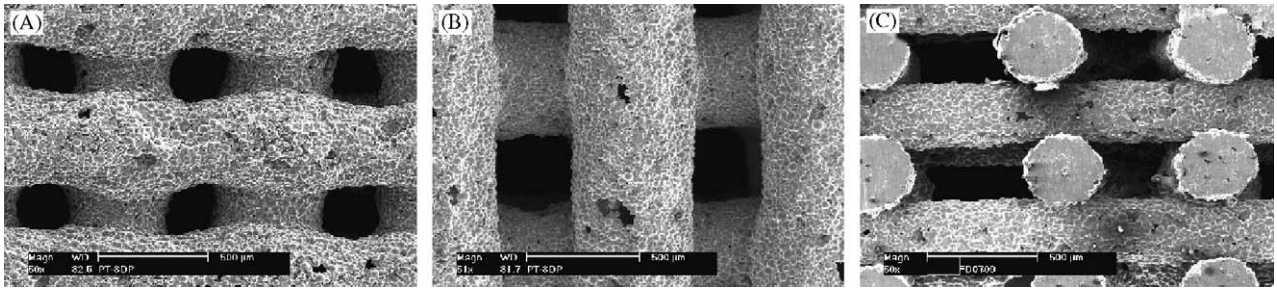

Fig. 4. Effect of concentration of powder on the scaffold processing. (A) Low concentration shows the fiber is deformed. (64 vol% Ti_6Al_4V powder used.) (B) Optimal concentration (66 vol%). (C) When the powder concentration is high (i.e. 68 vol% Ti_6Al_4V powder used), there is no adhesion and attachment between the layers.

to control the fiber depositing system to achieve the required speed and initial height of fiber depositing.

3.4. Air pressure, feeding speed and initial height on the scaffold structure

At constant flow rate, it is clear that with a relative low feeding speed rate too much slurry is deposited and the fiber starts to swell. In this case, the solution is to increase the feeding speed or to reduce the pressure slightly to change the flow rate. On the other hand, if the feeding speed is too fast, the fiber is stretched after it has been deposited and it touches the previous layer much later and affects the contact area between layers. Therefore the material flow rate through the nozzle and the feeding speed must be coordinated with each other. The optimum situation is when the material leaves the nozzle and is immediately pressed against and bonded to the fibers of the previous layer, being only slightly deformed. Fig. 6 shows the effect of air pressure on the scaffold processing at constant feeding speed. With low pressure, there is less adhesion and attachment between the layers (Fig. 6A); with higher pressures, the diameter of fiber becomes large (Fig. 6C); optimal air pressure causes the fibers to have a good attachment to each other with minimal deformation (Fig. 6B). In a similar way, the feeding speeds affect the scaffold structure at constant pressure as shown in Fig. 7. At low speed, the slurry flow rate from the nozzle is too high, and the scaffold becomes denser (Fig. 7A). At high feeding speed, the fibers become thinner (Fig. 7B–D), and dragging of the dispensed material from preceding fibers easily occurs. Table 1 shows the fiber diameter and total porosity of scaffold as function of the fiber depositing pressure and feeding speed. It can be seen that the diameter increased with pressure and decreasing of feeding speed, and the porosity of scaffold increased with the feeding speed and decreasing of pressure.

The initial height of the nozzle head above the platform is also important for scaffold construction. It was observed that a large initial height reduced the attachment area of the first layer with the platform, resulting in the instability of the scaffold during fiber depositing and the possible dragging of material. Conversely, a very low height made the first layer becomes denser because of the fibers being spread out to large diameters. Fig. 8 shows the effect of the initial distance between nozzle tip and platform on the scaffold processing.

The quality of the bonding between the layers is equally important. The thickness of layer in the Z-direction is of importance to guarantee the contact area between the fibers. Lander reported the thickness of a layer should be 80–90% of the diameter of the nozzle so that a sufficient contact area between the layers can be obtained to stick them together, and the material of the overlapping area is plotted lateral to the contact area [46]. Obviously, it is no use if the thickness is equal and larger than the diameter of fiber because the layers would only just touch, and the bonding is inadequate. If a too low thickness is chosen, the fibers are deformed in the overlapping area and the porosity drops considerably. With a nozzle diameter of 400 μm, a fiber depositing pressure (P) of 2.5 bars, feeding speed (F) of 350 mm/min and initial height of fiber depositing (H) of 0.25 mm, were found to be optimal for fabricating the scaffolds. Fig. 9 shows the resulting scaffold under these conditions.

3.5. Shrinkage of porous Ti_6Al_4V

Due to high concentration of powder in the slurry almost up to maximum packing density, the shrinkage of sample after drying is neglectable. During sintering, however, shrinkage occurs due to interfusion (necking) of the spherical particles. A sample measuring $20 \times 20 \times 10$ mm before sintering measured $19.2 \times 19.15 \times 9.1$ mm after sintering under 1250 °C for 2 h. Consequently, the horizontal linear shrinkage is about 8.5% and the vertical linear shrinkage 9%, corresponding to a volumetric decrease of 16.5%.

3.6. Macrostructure and microstructure

The macrostructure of the scaffolds obtained by 3D fiber depositing presents a fully interconnected pore network (Fig. 9A). The microstructure of a separate fiber is shown in Fig. 10A. It shows that particle bonding is achieved by neck growth through a solid-state diffusion process. The

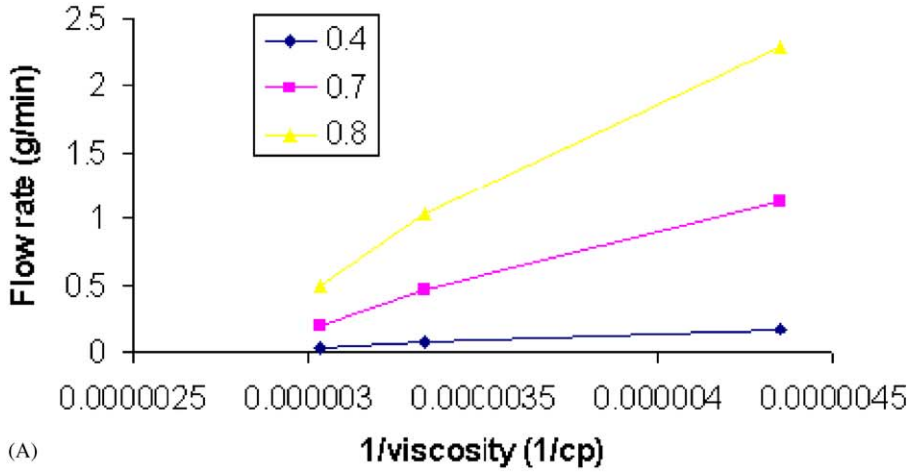

(A)

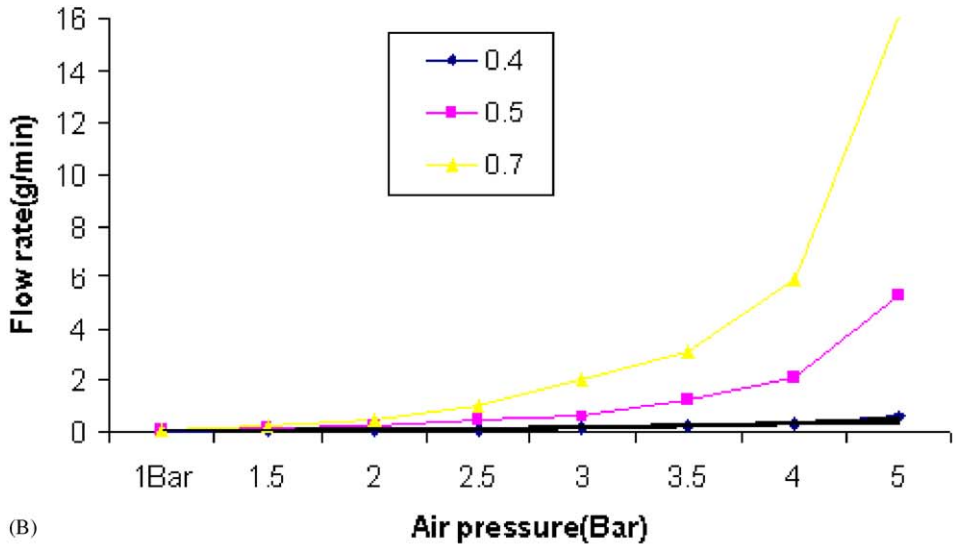

(B)

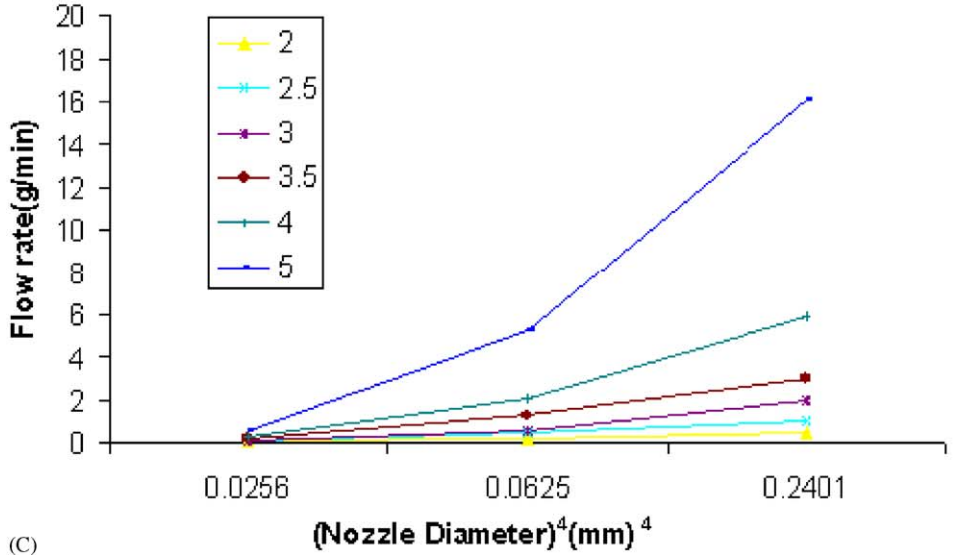

(C)

Fig. 5. The flow rate as a function of 1/viscosity, pressure and (nozzle diameter)^4. (A) Flow rate varied with 1/viscosity at a nozzle diameter of 0.4 mm and a pressure of 2.5 bar, (B) Flow rate varied with (nozzle diameter)^4 at different pressure, (C) Flow rate varied with pressure with different nozzle diameter.

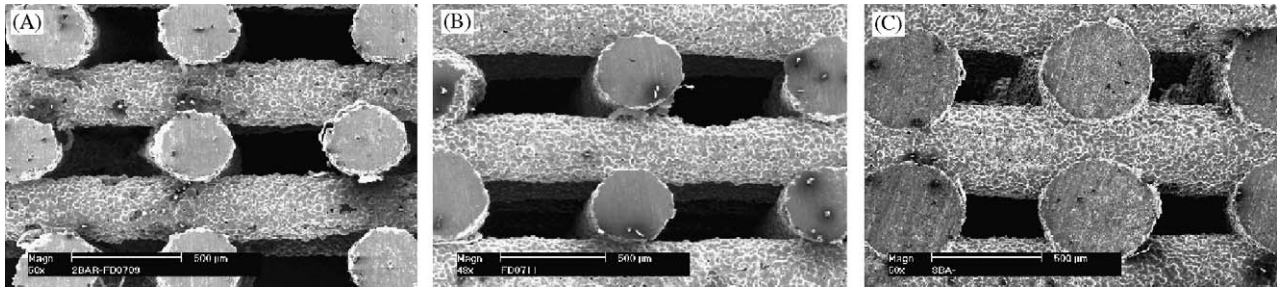

Fig. 6. Effect of fiber depositing pressure on the scaffold processing. (A) 2 Bar, (B) 2.5 Bar, (C) 3 Bar.

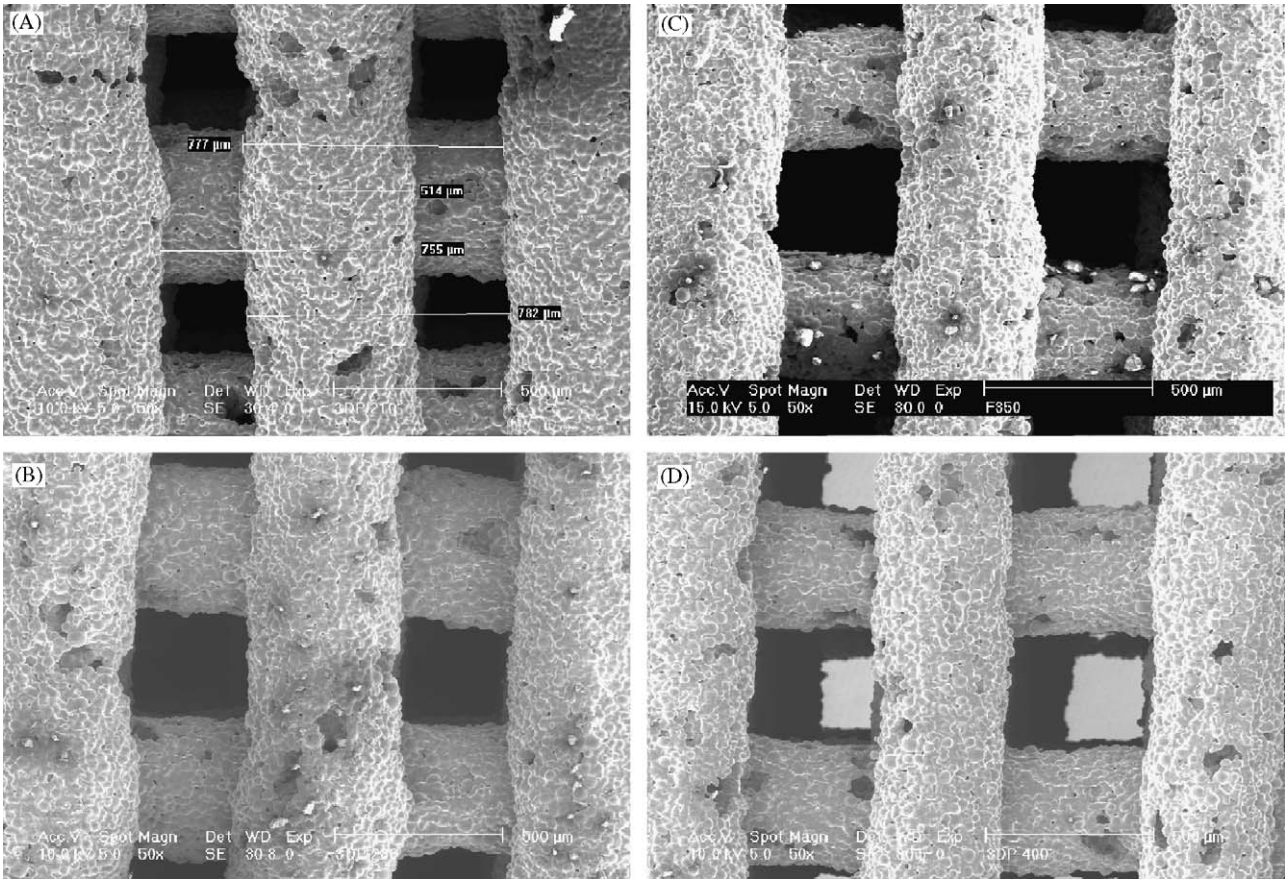

Fig. 7. Effect of feeding speed on the scaffold processing. (A) 210 mm/min, (B) 280 mm/min, (C) 350 mm/min, (D) 420 mm/min.

Table 1
Measurement of Ti_6Al_4V scaffold by different pressure and feeding speed from ESEM micrographs

Specimen group	FD	FS	Porosity
F-210	518±21.5	249±9.9	50±2
F-280	454±12.7	339±12.3	54±1
F-350	415±14.9	369±11.9	58±1
F-400	364±10.3	419±33.5	64±1.5
P-2 Bar	320±6.9	477±7.4	74±1
P-2.5 Bar	415±14.9	369±11.9	58±1
P-3 Bar	477±4.4	352±4.9	49±2

FD: Fiber diameter, FS: Fiber spacing, P: porosity.

formation of necks between particles is evidence of good sintering conditions. It can be seen that both macro and micro pores exist in the scaffold. Macro pores are generated and controlled by fiber spacing and layer thickness. Micro pores are left after powder sintering. ESEM shows that the micropore size ranges from 1–10 μm. Fig. 10B shows a cross-section that reveals attachment between layers of the scaffold, as a result of the solid diffusion process. The dimensions as shown in Table 1 prove that fiber diameter, fiber space and porosity have little variation. It means that the scaffold made by 3D fiber deposition possess a uniform structure.

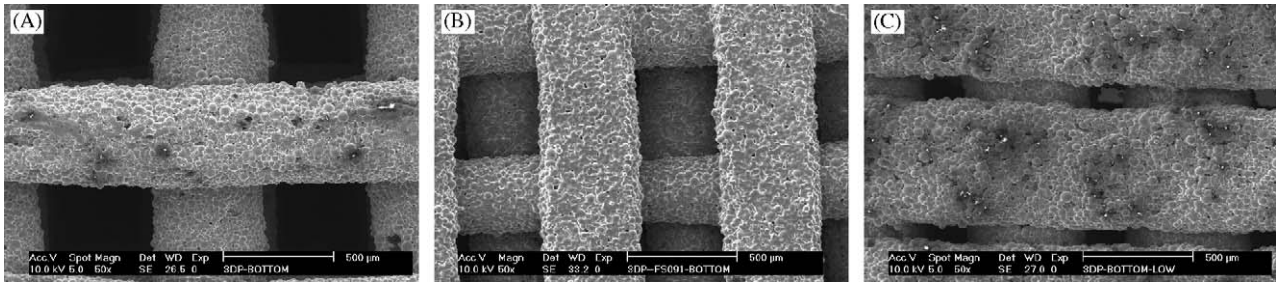

Fig. 8. Effect of the initial height of nozzle head and platform on the scaffold processing. (A) Initial height is 0.4 mm, (B) initial height is 0.25 mm, (C) initial height is 0.1 mm.

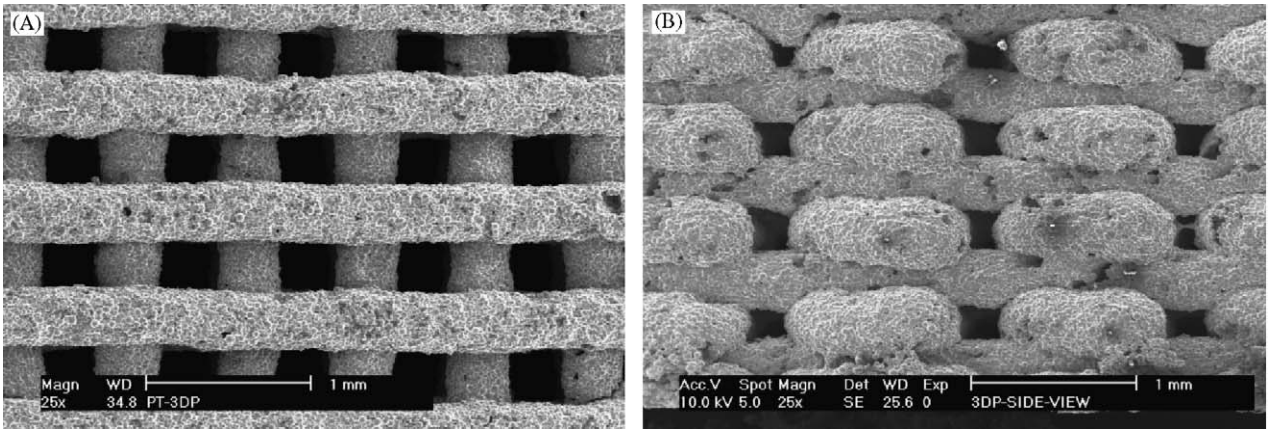

Fig. 9. Ti_6Al_4V scaffold by 3D fiber depositing. (A) Top view, (B) side view.

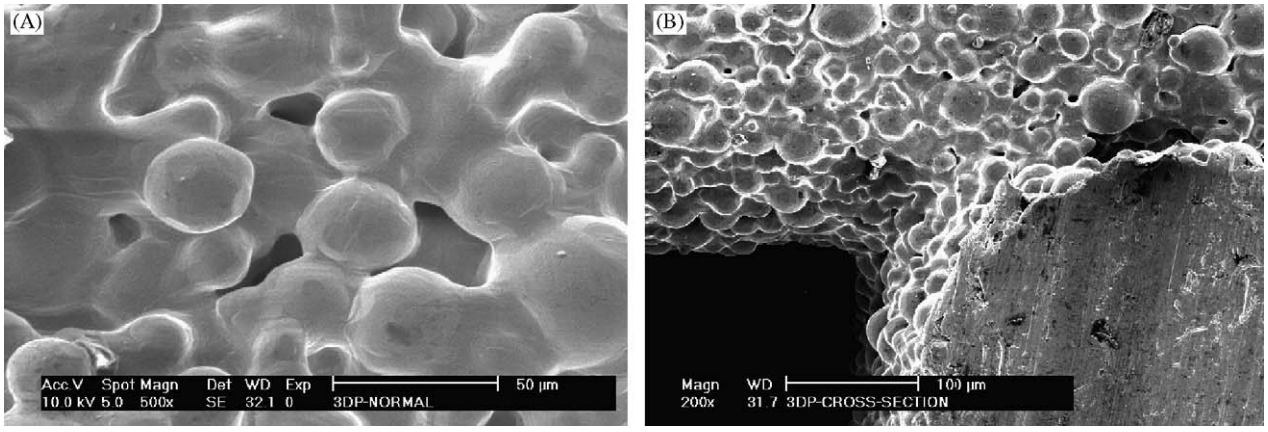

Fig. 10. Microstructure of 3D porous Ti_6Al_4V. (A) High magnification of fiber surface, (B) interface between layers.

3.7. Mechanical properties

The compressive strength of scaffolds made with different pressure and feeding speed is shown in Fig. 11. It can be seen that the compressive strength increases with the pressure (Fig. 11A) and decreases with increasing feeding speed (Fig. 11B). As shown in Table 1, the porosity of scaffold was changed by different pressure and feeding speed. Therefore, the compressive strength was affected by porosity. It is in agreement with Gibson and Ashby's model which the stress varies with porosity [65].

3.8. In vitro experiment

Fig. 12 shows ESEM images of cells cultured on the porous Ti_6Al_4V samples for 1 day (Fig. 12A), 3 days (Fig. 12B) and 7 days (Fig. 12C). Polygonal and spindle-shaped cells attached and spread on porous surface of the

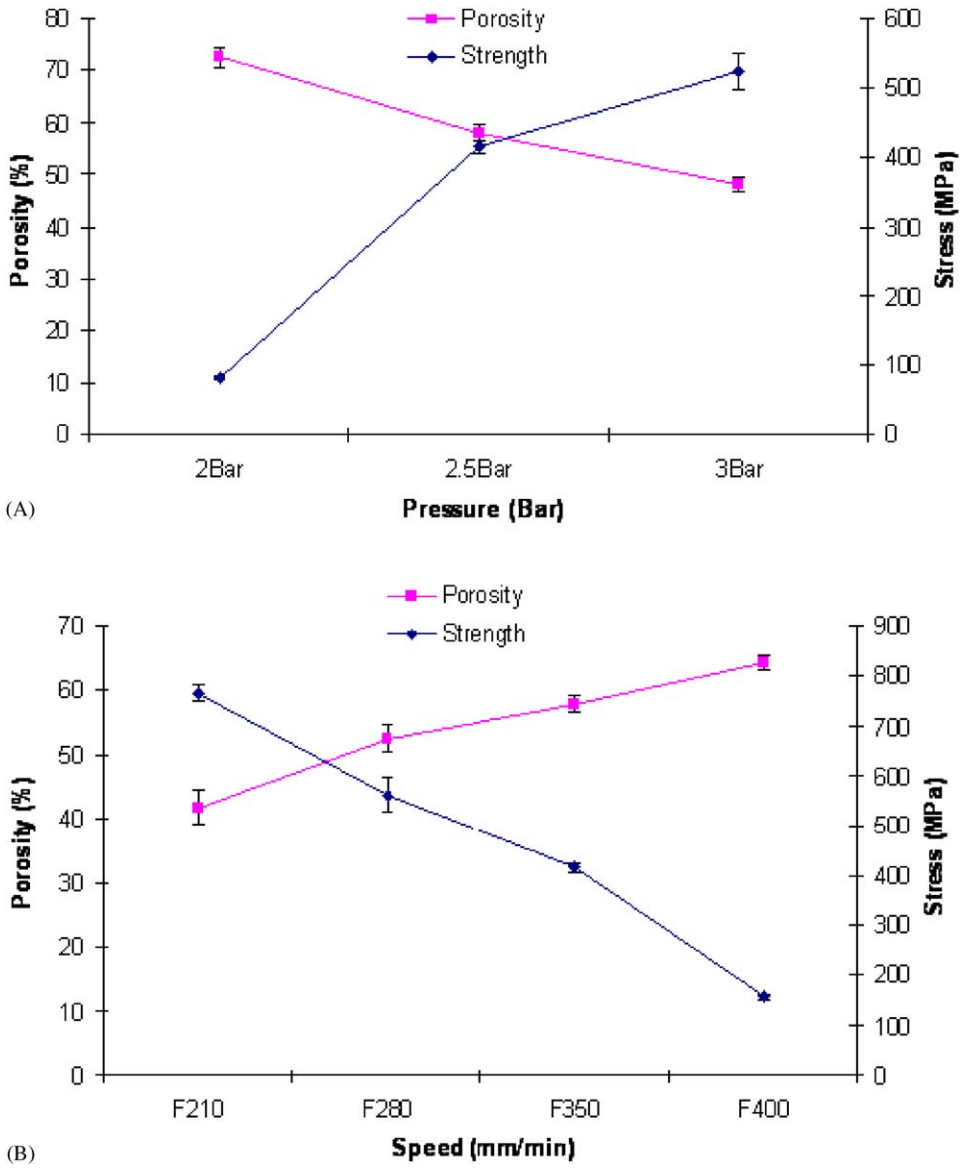

Fig. 11. Compressive strength of scaffold varied with different pressure and feeding speed. (A) Compressive strength as function of air pressure, (B) Compressive strength as function of feeding speed.

fibers. Also some cells were found growing via micropores into the inner surface. The spreading cells maintained a physical contact with each other by lamellopodia. Significant cell growth was found over culture period of 7 days. After 1 day culture, only a few cells were seen on the surface (Fig. 12A), however, increasing amounts of cells were found after 3 days and 7 days culture (Fig. 12B and C), A DNA content assay (Table 2, $R^2 = 0.99$) also confirmed that with increasing of culture time, more cells were found to attach and spread on the 3D porous scaffold.

Fig. 13A shows amount of protein produced by osteoblast-like cells. The amount of protein increased with the incubation of time. The ALP/DNA activity of cell layers grown on the 3D fiber scaffold also increased as function of seeding time (Fig. 13B). The results in vitro show that the cells are not only able to attach and spread well on the surface of porous Ti_6Al_4V fibers, but also be able to form an extracellular matrix on the surface (Fig. 13).

4. Discussion

4.1. Ti_6Al_4V powder

The used Ti_6Al_4V powder shows applicability for fiber depositing 3D scaffold. There are four reasons for choosing this powder system. First, the broad distribution of particle size allows a high packing density of powders so that slurries with higher concentrations of powder can be

prepared [66]. The optional concentration of powder in the slurry was found to be high as compared to some metal slurries such as with stainless steel (56 vol%) [66]. Second, the small powder diameter allows for using small diameter nozzle and reduction of minimum thickness of layer. Third, fine powders can be sintered more readily than coarse ones due to large surface area [67,68]. Finally, the smooth surface of the particles will enhance powder flowability enabling them to readily flow through small nozzle head without blocking [69].

4.2. Slurry

A high viscosity of the slurry is unavoidable at the concentration levels necessary for enough consistency immediately after extrusion and acceptable shrinkage percentage during drying and sintering. Too high viscosity, on the other hand, will hamper the flow of the slurry through fine nozzles. Fortunately, these slurries show thixotropic behavior, meaning lower apparent viscosity at high shear rates, thus facilitating flow through the nozzle canal, when, after extrusion the slurry is at rest and zero shear rate, the viscosity increases giving the extra enough consistency to prevent flow under gravity force.

4.3. Advantages of 3D fiber depositing porous Ti_6Al_4V

Several significant advantages of 3D fiber depositing over other processes in porous scaffold fabrication include:

(1) Ti_6Al_4V scaffolds can be fabricated directly by 3D fiber deposition. It is easy to produce complex geometry with small dimensional defects, which is difficult with casting or milling of titanium, by the setting of parameters, such as fiber spacing, layer thickness and fiber direction. Meanwhile, the nozzles of this fiber depositing system are derived from hypodermic needles and thus disposable, and very cheap. Different diameters of these nozzles are readily available. Therefore, it is possible to assign nozzles of different diameter to different parts to make a functional scaffold.

(2) In most methods of RP, special support structures are needed to support overhanging features of the scaffold. For powder-based methods, like selective laser sintering (SLS) and 3D printing, no support structures are typically required to create complex shapes. But in these methods powder is locally consolidated and the remaining powders serve as support for over hanging structure [34,70]. It is obvious that the support powder in the inner structure is difficult to be removed completely later. SEM images showed that

Table 2
DNA content of cells attached on the porous Ti_6Al_4V

Cultured time (days)	DNA content (ng)
1	475±36
3	1308±105
7	2307±87

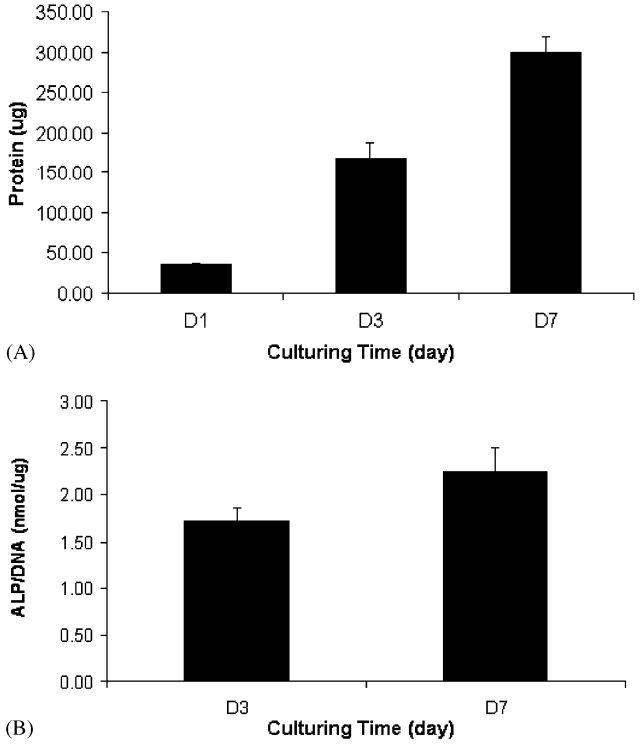

Fig. 13. (A) Protein content of MC3T3-E1 osteoblast-like cells grown on porous Ti_6Al_4V scaffold varied with the culturing time, (B) ALP/DNA activity of MC3T3-E1 monitored on the scaffold of 3days and 7days.

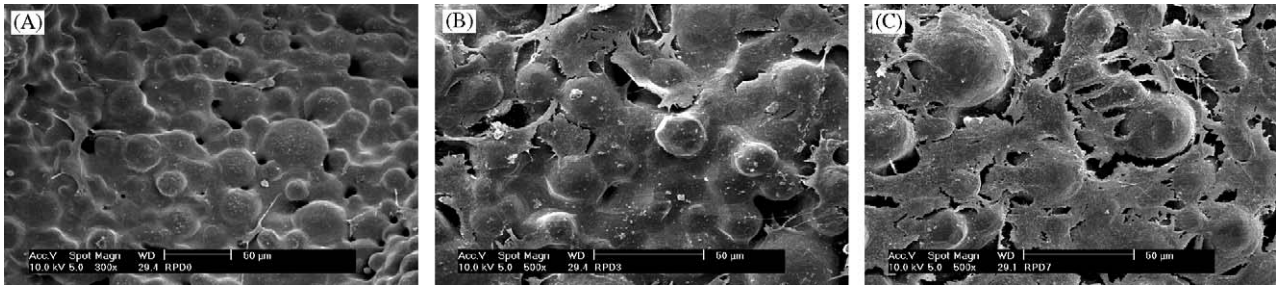

Fig. 12. Morphology of MC3T3-E1osteoblast-like cells cultured on the porous Ti_6Al_4V for (A) 1 day, (B) 3 days, (C) 7 days.

the deposited Ti_6Al_4V fibers were able to suspend themselves as overhanging fibers with little or no slack (Fig. 5). It reveals that these fibers after depositing and solidifying have sufficient strength to hold the shape.

(3) There are some limitations for the variety of materials in conventional RP systems [70,71]. The fiber depositing system described here maybe operated at both high temperature and room temperature offering the versatility and possibility to apply a wide variety of materials, such as polymers, metal, ceramics and multiple material combinations.

4.4. Limitations of 3D fiber depositing porous Ti_6Al_4V

Firstly, there is a lower limit of the nozzle size. According to the Hagen–Poiseuille equation, a minor decrease in nozzle diameter will dramatically decrease flow rate and require considerably, greater pressures to deposit suitable fibers. For very small nozzle diameter, even complete blocking of the flow by bridge forming of the particles can be expected. Second, the deposited structures will show some anisotropy, the pore size in Z-direction is not necessarily the same as that in x- and y-directions but depends on the thickness of the layers. Finally, some pore occlusion at boundaries may occur because of fiber depositing path (Fig. 9B) due to continuous fiber depositing.

5. Conclusion

Porous Ti_6Al_4V scaffolds were successfully fabricated directly by a rapid prototyping technique, 3D fiber deposition. It is shown that Ti_6Al_4V slurry is a key point for building 3D scaffolds. Three main parameters of the fiber depositing process: the dispensing pressure, feeding speed and initial height between nozzle and platform were investigated for its effect on the integrity of scaffold fabricated. Through a series of experiments, for a nozzle diameter of 0.4 mm, a powder concentration of 66 vol%, a fiber depositing pressure of 2.5 bar, a feeding speed of 350 mm/min and an initial height 0.25 mm, were found to be optimal for fabrication of Ti_6Al_4V scaffolds. The scaffolds have a good attachment between layers, and a fully interconnected porous structure. By varying the direction of fiber depositing and the space between the fibers, scaffolds with highly uniform internal honeycomb-like structures, controllable pore morphology and complete pore interconnectivity can be obtained. Results of in vitro studies revealed the biocompatibility of these scaffolds, which are not only non-toxic but also favorable for cell attachment, proliferation and differentiation. The results of this study demonstrate the potential application in rapid fabrication of 3D Ti_6Al_4V scaffolds with regular and reproducible architecture for tissue engineering scaffolds and orthopedic implants.

Acknowledgments

The authors thank Lorenzo Moroni for his enthusiastic help in the 3D-fiber depositing. The discussions with Dr. Huipin Yuan were very constructive during the preparation of this paper.

Reference

[1] Vacanti JP, Vacanti CA. The history and scope of tissue engineering, in principles of tissue engineering. 2nd ed. New York: Academic Press; 2000. p. 3–8.

[2] Yang S, Leong KF, Du Z, Chua CK. The design of scaffolds for use in tissue engineering. Part I. traditional factors. Tissue Eng 2001;7(6): 679–89.

[3] Hollister S, Lin C, Saito E, Schek R, Taboas J, Williams J, et al. Engineering craniofacial scaffolds. Orthod Craniofac Res 2005;8(3): 162–73.

[4] Chang BS, Lee CK, Hong KS, Youn HJ, Ryu HS, Chung SS, et al. Osteoconduction at porous hydroxyapatite with various pore configurations. Biomaterials 2000;21(12):1291–8.

[5] Nagashima T, Ohshima Y, Takeuchi H. Osteoconduction in porous hydroxyapatite ceramics grafted into the defect of the lamina in experimental expansive open-door laminoplasty in the spinal canal. Nippon Seikeigekagakkai Zasshi 1995;69(4):222–30.

[6] Tamai N, Myoui A, Tomita T, Nakase T, Tanaka J, Ochi T, et al. Novel hydroxyapatite ceramics with an interconnective porous structure exhibit superior osteoconduction in vivo. J Biomed Mater Res 2002;59(1):110–7.

[7] Simske SJ, Ayers RA, Bateman TA. Porous materials for bone engineering. Mater Sci Forum 1997;250:151–82.

[8] Ciapetti G, Ambrosio L, Savarino L, Granchi D, Cenni E, Baldini N, et al. Osteoblast growth and function in porous poly epsilon - caprolactone matrices for bone repair: a preliminary study. Biomaterials 2003;24(21):3815–24.

[9] Du C, Meijer GJ, van de Valk C, Haan RE, Bezemer JM, Hesseling SC, et al. Bone growth in biomimetic apatite coated porous Polyactive 1000PEGT70PBT30 implants. Biomaterials 2002;23(23): 4649–56.

[10] Kalita SJ, Bose S, Hosick HL, Bandyopadhyay A. Development of controlled porosity polymer-ceramics composite scaffolds via fused deposition modeling. Mater Sci Eng (C) 2003;23:611–20.

[11] Zhang R, Ma PX. Poly(*a*-hydroxyl acids)/hydroxyapatite porous composites for bone-tissue engineering. I. Preparation and morphology. J Biomed Mater Res 1999;44:446–55.

[12] Williams DF. Titanium in medicine. Heidelberg, Germany: Spinger; 2001 13p..

[13] Wen C, Yamata Y, Mabuchi M. Processing and mechanical properties of autogenous titanium implant materials. J Mater Sci: In Medicine 2002;13:397–401.

[14] Holtorf HL, Jansen JA, Mikos AG. Ectopic bone formation in rat marrow stromal cell/titanium fiber mesh scaffold constructs: effect of initial cell phenotype. Biomaterials 2005;26(31):6208–16.

[15] Walboomers XF, Jansen JA. Bone tissue induction, using a COLLOSS-filled titanium fibre mesh-scaffolding material. Biomaterials 2005;26(23):4779–85.

[16] Lueck RA, Galante JO, Rostoker W, Ray RD. Development of an open pore metallic implant to permit attachment to bone. Surg Forum 1969;20:456–7.

[17] Welsh RP, Pilliar RM, Macnab I. Surgical implants. The role of surface porosity in fixation to bone and acrylic. J Bone J Surg Am 1971;53(5):963–77.

[18] Hahn H, Palich W. Preliminary evaluation of porous metal surfaced titanium for orthopedic implants. J Biomed Mater Res 1970;4(4): 571–7.

[19] Wu BD, Cui YF. Research on porous titanium for medical implant material. Rare Metal Mater Eng 1988;4.
[20] Fujibayashi S, Neo M, Kim HM, Kokubo T, Nakamura T. Osteoinduction of porous bioactive titanium metal. Biomaterials 2004;25(3):443–50.
[21] Galante J, Rostoker W. Fiber metal composities in the fixation of skeletal prosthesis. J Biomed Mater Res 1973;4:43–61.
[22] Galante J, Rostoker W, Lueck R. Sintered fibre metal composites as a basis for attachment of implants to bone. J Bone J Surg 1971;53A(1): 101–14.
[23] Davis NG, Teisen J, Schuh C, Dunand DC. Solid-state foaming of titanium by superplastic expansion of argon-filled pores. J Mater Res 2001;16:1508–39.
[24] Li JP, Li SH, Van Blitterswijk CA, De Groot K. A novel porous Ti_6Al_4V: characterization and cell attachment. J Biomed Mater Res 2005;73A:223–33.
[25] Yang S, Leong KF, Du Z, Chua CK. The design of scaffolds for use in tissue engineering. Part II. Rapid prototyping techniques. Tissue Eng 2002;8(1):1–11.
[26] Sachlos E, Czernuszka JT. Making tissue engineering scaffolds work. Review: the application of solid freeform fabrication technology to the production of tissue engineering scaffolds. Eur Cell Mater 2003;5:29–39 [discussion 39–40].
[27] Sachlos E, Reis N, Ainsley C, Derby B, Czernuszka JT. Novel collagen scaffolds with predefined internal morphology made by solid freeform fabrication. Biomaterials 2003;24(8):1487–97.
[28] Webb PA. A review of rapid prototyping (RP) techniques in the medical and biomedical sector. J Med Eng Technol 2000;24(4):149–53.
[29] Hollister SJ. Porous scaffold design for tissue engineering. Nat Mater 2005;4(7):518–24.
[30] Yeong WY, Chua CK, Leong KF, Chandrasekaran M. Rapid prototyping in tissue engineering: challenges and potential. Trends Biotechnol 2004;22(12):643–52.
[31] Hutmacher DW, Sittinger M, Risbud MV. Scaffold-based tissue engineering: rationale for computer-aided design and solid free-form fabrication systems. Trends Biotechnol 2004;22(7):354–62.
[32] Hutmacher DW. Scaffolds in tissue engineering bone and cartilage. Biomaterials 2000;21(24):2529–43.
[33] Hutmacher DW. Scaffold design and fabrication technologies for engineering tissues—state of the art and future perspectives. J Biomater Sci Polym Ed 2001;12(1):107–24.
[34] Seitz H, Rieder W, Irsen S, Leukers B, Tille C. Three-dimensional printing of porous ceramic scaffolds for bone tissue engineering. J Biomed Mater Res B: Appl Biomater 2005;74B(2):782–8.
[35] Tan KH, Chua CK, Leong KF, Naing MW, Cheah CM. Fabrication and characterization of three-dimensional poly(ether-ether-ketone)/-hydroxyapatite biocomposite scaffolds using laser sintering. Proc Inst Mech Eng (H) 2005;219(3):183–94.
[36] Dhariwala B, Hunt E, Boland T. Rapid prototyping of tissue-engineering constructs, using photopolymerizable hydrogels and stereolithography. Tissue Eng 2004;10(9–10):1316–22.
[37] Woodfield TB, Malda J, de Wijn J, Peters F, Riesle J, van Blitterswijk CA. Design of porous scaffolds for cartilage tissue engineering using a three-dimensional fiber-deposition technique. Biomaterials 2004;25(18):4149–61.
[38] Wilson CE, de Bruijn JD, van Blitterswijk CA, Verbout AJ, Dhert WJ. Design and fabrication of standardized hydroxyapatite scaffolds with a defined macro-architecture by rapid prototyping for bone–tissue-engineering research. J Biomed Mater Res A 2004;68(1): 123–32.
[39] Zein I, Hutmacher DW, Tan KC, Teoh SH. Fused deposition modeling of novel scaffold architectures for tissue engineering applications. Biomaterials 2002;23(4):1169–85.
[40] Curodeau A, Sachs E, Caldarise S. Design and fabrication of cast orthopedic implants with freeform surface textures from 3-D printed ceramic shell. J Biomed Mater Res 2000;53(5):525–35.
[41] Melican MC, Zimmerman MC, Dhillon MS, Ponnambalam AR, Parsons JR. Three-dimensional printing and porous metallic surfaces: a new orthopedic application. J Biomed Mater Res 2001;55(2): 94–202.
[42] Wu M, Tinschert J, Augthun M, Wagner I, Schadlich-Stubenrauch J, Sahm PR, et al. Application of laser measuring, numerical simulation and rapid prototyping to titanium dental castings. Dent Mater 2001;17(2):102–8.
[43] Mazumder J, Dutta JD, Kikuchi N, Ghosh A. Closed loop direct metal deposition: art to part. Opt Lasers Eng 2000;34: 397–414.
[44] Mazumder J, Qi H. Fabrication of 3D components by laser-aided direct metal deposition. In: Thomas Schriempf J, editor. Proceedings of the International Society for Optical Engineering. V 5706. San Jose, CA, USA, 2005, p. 38–59.
[45] Landers R, Hubner U, Schmelzeisen R, Mulhaupt R. Rapid prototyping of scaffolds derived from thermoreversible hydrogels and tailored for applications in tissue engineering. Biomaterials 2002;23(23):4437–47.
[46] Landers R, pfister A, John H, Hubner U, Schmelzeisen R, Mulhaupt R. Fabrication of soft tissue engineering scaffolds by means of rapid prototyping techniques. J Mater Sci 2002;37:3107–16.
[47] Klawitter JJ, Hulbert SF. Application of porous ceramics for the attachment of load bearing orthopedic applications. J Biomed Mater Res Symp 1971;2:161–7.
[48] Bobyn JD, Pilliar RM, Cameron HU, Weatherly GC. The optimum pore size for the fixation of porous-surfaced metal implants by the ingrowth of bone. Clin Orthop 1980;150:263–70.
[49] Yuan H, Kurashina K, de Bruijn JD, Li Y, de Groot K, Zhang X. A preliminary study on osteoinduction of two kinds of calcium phosphate ceramics. Biomaterials 1999;20(19):1799–806.
[50] Bose S, Darsell J, Hosick HL, Yang L, Sarkar DK, Bandyopadhyay A. Processing and characterization of porous alumina scaffolds. J Mater Sci Mater Med 2002;13(1):23–8.
[51] Hutmacher DW, Schantz T, Zein I, Ng KW, Teoh SH, Tan KC. Mechanical properties and cell cultural response of polycaprolactone scaffolds designed and fabricated via fused deposition modeling. J Biomed Mater Res 2001;55(2):203–16.
[52] Yedavalli RV, Loth F, Yardimci A, Pritchard WF, Oshinski JN, Sadler L, et al. Construction of a physical model of the human carotid artery based upon in vivo magnetic resonance images. J Biomech Eng 2001;123(4):372–6.
[53] Comb JW, Priedeman WR, Turley PW. Layered manufacturing control parameters and material selection criteria. New York: Manufacturing Science and Engineering, Production Engineering Division, ASME; 1994. p. 547–56.
[54] Yardimci AM, Guceri SI, Danforth SC, Agarwala M, Safari A. Numerical modelling of fused deposition modelling, Part 2. San Francisco, USA, 1995.
[55] Lowry OH. Micromethods for assay of enzyme. II. Specific procedures. Alkaline phosphatase, 1955. 371p.
[56] Boyan BD, Bonewald LF, Swain LD. Localization of 1,25-(OH)2 D3 responsive alkaline phosphatase in osteoblast-like cells (ROS 17/2,8, MG 63., and MC 3T3) and growth cartilage cells in culture. J Biol Chem 1989;264:11879.
[57] Bretaudiere JP, Spillman T. Alkaline phosphatase. In: Methods of enzymatic analysis. Weinheim, Germany: Verlag Chemica; 1984. p. 75–92.
[58] Liu Y, Hunziker EB, de Groot K. BMP-2 incorporated into biomimetic coatings retains its biological activity. Tissue Eng 2004;10.
[59] Landers R, Mulhaupt R. Desktop manufacturing of complex objects, prototypes and biomedical scaffolds by means of computer-assisted design combined with computer-guided 3D plotting of polymers and reactive oligomers. Macromol Mater Eng 2000;282:17–21.
[60] More solutions to sticky problems—a guide to getting more from your Bronkfield viscometer. US: Brookfield Engineering Labs., Inc., 2000. 16p.
[61] Benhow J, Bridgwater J. Pater flow and extrusion. Oxford: Clarendon Press; 1993.

[62] Grida I, Evans JRG. Extrusion freeforming of ceramics through fine nozzles. J Eur Ceram Soc 2003;23:629–35.
[63] Rangarajan S, Qi G, Venkataraman N, Safari A, Danforth SC. Powder processing, rheology, and mechanical properties of feedstock for fused deposition of Si3N4 ceramic. J Am Ceram Soc 2000;83(7): 1663–9.
[64] Vozzi G. Microsyringe-based deposition of two-dimensional and three-dimensional polymer scaffolds with a well-defined geometry for application to tissue engineering. Tissue Eng 2003;8(6):1089–98.
[65] Gibson LJ, Ashby MF. Cellular solids: structure and properties. Cambridge: Cambridge University Press; 1997.
[66] Liao J, Zhang B. Porous materials of powder metallurgy. China: Metallurgy Industry Press; 1978.
[67] Oh IH, Nomura N, Masahashi N. Mechanical properties of porous titanium compacts prepared by powder sintering. Scr Mater 2003;49: 1197–202.
[68] Mu W, Deng GZ, Luo FC. Titanium metallurgy. Beijing: Metallurgy Industry Press; 1998.
[69] Hong SB, Eliaz N, Leisk GG, Sach EM, Latanision RM, Allen SM. A new Ti-5Ag alloy for customized prostheses by three-dimensional printing (3DP). J Dent Res 2001;80(3):860–3.
[70] Leong KF, Cheah CM, Chua CK. Solid freeform fabrication of three-dimensional scaffolds for engineering replacement tissues and organs. Biomaterials 2003;24(13):2363–78.
[71] Lee M, Dunn JC, Wu BM. Scaffold fabrication by indirect three-dimensional printing. Biomaterials 2005;26(20):4281–9.